ELSEVIER

Journal of Biomechanics 40 (2007) 2580–2585

JOURNAL OF BIOMECHANICS

www.elsevier.com/locate/jbiomech
www.JBiomech.com

Short Communication

Stent expansion in curved vessel and their interactions: A finite element analysis

Wei Wu*, Wei-Qiang Wang, Da-Zhi Yang, Min Qi

Department of Materials Engineering, Dalian University of Technology, No. 2, LingGong Road, Dalian, LiaoNing 116024, China

Accepted 17 November 2006

Abstract

Coronary restenosis after angioplasty has been reduced by stenting procedure, but in-stent restenosis (ISR) has not been eliminated yet, especially in tortuous vessels. In this paper, we proposed a finite element method (FEM) to study the expansion of a stent in a curved vessel (the CV model) and their interactions. A model of the same stent in a straight vessel (the SV model) was also studied and mechanical parameters of both models were researched and compared, including final lumen area, tissue prolapse between stent struts and stress distribution. Results show that in the CV model, the vessel was straightened by stenting and a hinge effect can be observed at extremes of the stent. The maximum tissue prolapse of the CV model was more severe (0.079 mm) than the SV model (0.048 mm); and the minimum lumen area of the CV was decreased (6.10 mm^2), compared to that of the SV model (6.28 mm^2). Tissue stresses of the highest level were concentrated in the inner curvature of the CV model. The simulations offered some explanations for the clinical results of ISR in curved vessels and gave design suggestions of the stent and balloon for tortuous vessels. This FEM provides a tool to study mechanisms of stents in curved vessels and can improve new stent designs especially for tortuous vessels.

Keywords: Curved vessel; Coronary stent; Finite element methods; In-stent restenosis; Mechanical properties

1. Introduction

In-stent restenosis (ISR) still remains an obsession to cardiologists (Mitra and Agrawal, 2006) even though drug-eluting stents are shown to improve stenting treatment (Tanabe et al., 2003). Stent–vessel interactions are considered as a controlling factor of ISR (Zhou et al., 2003), especially in tortuous vessels (Colombo et al., 2002). For the interactions of stents in curved vessels, a few in vivo (Abhyankar et al., 1997; Zhu et al., 2003) and in vitro (Kalmar et al., 2002; Rieu et al., 2003) studies have been done. However, these works just described clinical results or measured conformability of stents, and mechanics of stent deformation in curved vessels have not been discussed. Finite element methods (FEMs) are considered to be an efficient way of testing and improving stent designs to minimize ISR from biomechanical aspects (Prendergast et al., 2003; Brand and Ryvkin, 2005; Holzapfel et al., 2005; Lally et al., 2005; Wang et al., 2006) or fluid dynamics (Natarajan and Mokhtarzadeh-Dehghan, 2000; Wentzel et al., 2000; Chen et al., 2005; LaDisa et al., 2005; Johnston et al., 2006); however, stenting in curved vessels has seldom been modeled yet. This work proposed a FEM to describe the expansion of a stent in a curved vessel (the CV model) and their interactions. For comparison, the same stent was expanded in a straight vessel (the SV model). With the simulations, we expect to offer some explanations for ISR in curved vessels through biomechanical view and try to explain the results in terms of the model physics.

2. Materials and methods

2.1. Geometry models and material properties

The geometrical models were generated using Pro/Engineer (Parametric Technology Corporation) and were transformed into FEM code ANSYS (ANSYS, Inc.) for analysis. Both SV and CV models have four

*Corresponding author. Tel.: +86 411 84708441; fax: +86 411 84709284.
E-mail address: keyiyizhan@gmail.com (W. Wu).

0021-9290/$ - see front matter © 2006 Elsevier Ltd. All rights reserved.
doi:10.1016/j.jbiomech.2006.11.009

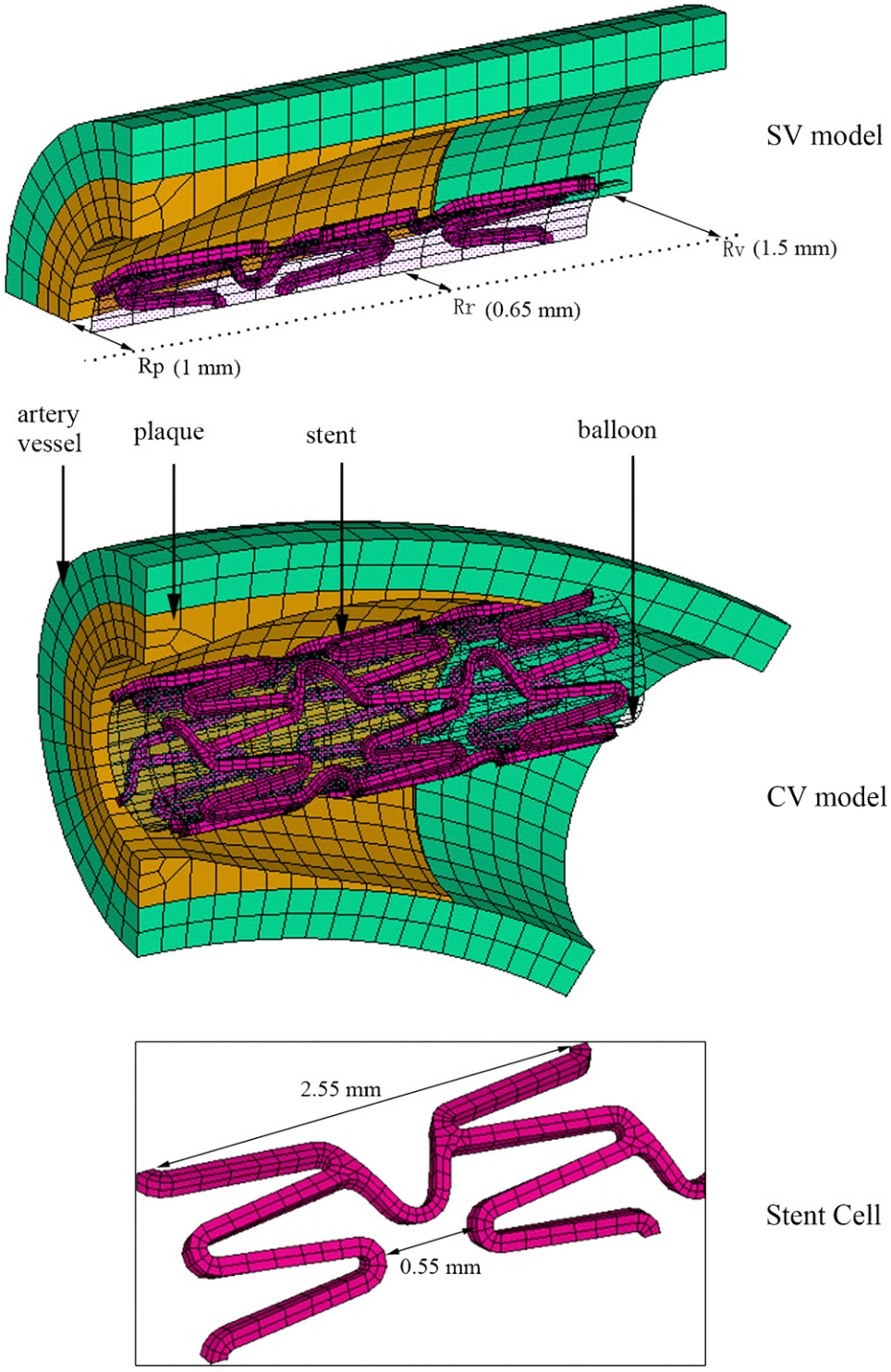

Fig. 1. Finite element models of the SV and CV model. The stent is our patent design, composed of struts with eight rings in circular direction, which are connected by four links in longitudinal direction; and the stent has a length of 9 mm, a thickness of 0.1 mm and an outer diameter of 1.5 mm. The struts will support the vessel and the links provide the stent flexibility for curved vessels. The width of struts and links is 0.1 mm. The sizes of a stent cell are also shown. The balloon was modeled as a rigid body and has a radius $R_r = 0.65$ mm and a length of 10 mm. In the SV model, the vessel has an inner radius $R_v = 1.5$ mm, a thickness of 0.5 mm and a length of 12 mm; the plaque has a length of 8 mm and was constructed through uniform rational B-splines and becomes thinner from middle to extreme parts. With its smallest inner radius $R_p = 1$ mm, the plaque corresponds to the severest stenosis of 56% for the reference vessel lumen area (7.07 mm^2). In the CV model, the lengths of the axes are 8 and 12 mm for the curved plaque and vessel, respectively; the diameters from axes and thicknesses of the vessel and plaque are the same as the SV model. For symmetry reasons, only one-eighth of the SV model was built and one-half of the CV model was modeled (the tissue in the CV model is shown in half).

components: stent (Yang, 2001), artery vessel, plaque and balloon (see Fig. 1). To model the curved tissue in the CV model, the vessel and plaque were built coaxially with a curvature of 0.1 mm^{-1} (Liao et al., 2004) in local toroidal coordinate system (LTCS; see Fig. 2) (ANSYS documentations, 2004).

The vessel and plaque are modeled as hyperelastic materials using a four-parameter and a six-parameter Mooney–Rivlin hyperelastic constitutive equation, respectively (Table 1). The parameters were derived from test data reported previously (Lee, 2000). The stent material was 316 L stainless steel and a standard true stress/strain curve for an annealed material was used (Young's modulus $E = 201$ GPa, Poisson ratio $v = 0.3$ and yield stress of 280 MPa).

2.2. Meshing and boundary conditions

For both models, the stent was meshed with eight-node solid185 elements while the tissue was meshed with eight-node hyperelastic Hyper58 elements. Flexible–flexible contact pairs were created between outer surface of the stent and inner surfaces of the tissue. Rigid–flexible contact pairs were created between the balloon and inner surface of the stent. No friction was considered for any contact pair. A sensitivity test was performed to ensure enough meshing refinement.

Symmetric constraints were applied to corresponding symmetry planes (on the stent, vessel and plaque) and symmetry lines (on the balloon). The ends of vessel and balloon were constrained in the longitudinal direction. Rotation of all components was inhibited.

2.3. Loading and solutions

For the SV model, the diameter of the balloon was firstly increased to 3.3 mm and a pressure of 0.0133 MPa was loaded on the inner area of tissue to simulate the blood pressure in the vessel. After that, the balloon was retracted to its original shape.

For the CV model, stent extremes at outer curvature protrude into the vessel of original configuration (Fig. 1), so "element birth and death" was introduced in simulations. Firstly, contact elements of the stent and vessel were "killed" to inactivate their contact condition. Meanwhile, a pressure (0.2 MPa) was loaded on the inner face of the tissue to expand the vessel and separate it from the stent. Secondly, all "killed" elements were activated and the diameter of the balloon was increased to 3.3 mm, with the pressure decreased to 0.0133 MPa. Lastly, the balloon was retracted to its original diameter.

After simulations, the following aspects were collected: (1) deformation of both models, especially conformity of the stent to the vessel, (2) the minimum lumen area and the severest stenosis, (3) tissue prolapse between the struts, and (4) the first principal stress in the tissue.

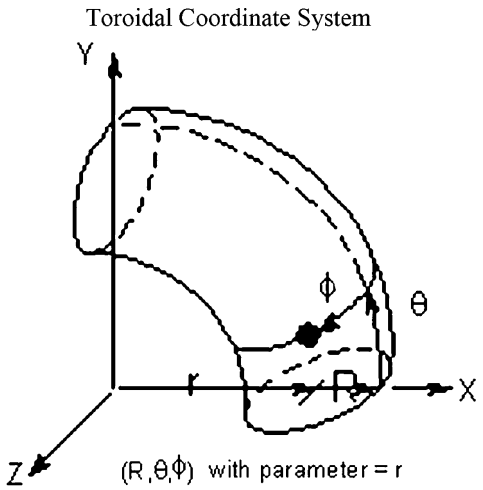

Fig. 2. The scheme of local toroidal coordinate system (LTCS). X, Y and Z correspond to R, θ and φ, respectively. For the CV model, the parameter r of the plaque and vessel is 10 mm.

Table 1
Hyperelastic Mooney–Rivlin constants to describe the materials of the vessel and plaque (in MPa)

	C1	C2	C3	C4	C5	C6
Vessel	0.020	0.003	0.175	0.090	—	—
Plaque	−0.452	0.510	0.101	1.256	0	0.301

3. Results

As Figs. 3a1 and a2 show, the stent in the SV model conformed to the vessel well during balloon expansion and retraction. However, the stent in the CV model was non-conformable to the vessel, especially at its extremes: The stent thoroughly straightened the middle vessel with full balloon expansion (Fig. 3b1); and after balloon retraction, although the stent was bent by the curved tissue, the middle vessel was straightened (Figs. 3b2 and b3). Furthermore, insets of Fig. 3b2 show that the displacement of the vessel of outer curvature was abruptly changed at the stent extreme; while at inner curvature, the stent extreme departed from the vessel. The CV model had the maximum tissue prolapse of 0.079 mm between the struts, which is nearly twice as much as that of the SV model (0.048 mm). The SV model had larger final minimum lumen area of 6.28 mm^2 and the least severe stenosis of 11.2%, as compared to 6.10 mm^2 and 13.7% of the CV model, respectively.

The distribution of tissue stresses in the SV model was more uniform than that of the CV model (Fig. 4). The higher plaque stresses of the CV model were concentrated at inner curvature and the vessel at outer curvature had higher stresses with the stent extreme. The maximum stress on plaque of the CV model (2.777 MPa) was higher than that of the SV model (2.419 MPa). For the highest stress on vessel, the CV model had three times stress (0.514 MPa) as much as that of the SV model (0.174 MPa).

4. Discussion and conclusions

At stent extremes of the CV model, the curvature of the vessel was changed sharply, indicating previously reported hinge points of curved vessels after stenting (Phillips et al., 1997; Colombo et al., 2002; Liao et al., 2004). At hinge points, rigid stent extremes and flexible vessel caused abrupt changes in longitudinal stiffness at the outer curvature and can lead to restenosis at the stent extremes (Colombo et al., 2002). Moreover, the maximum vessel stress was also induced at hinge points and was much higher than that of the SV model. The stresses of high level induced in the tissue by stenting have more risk of

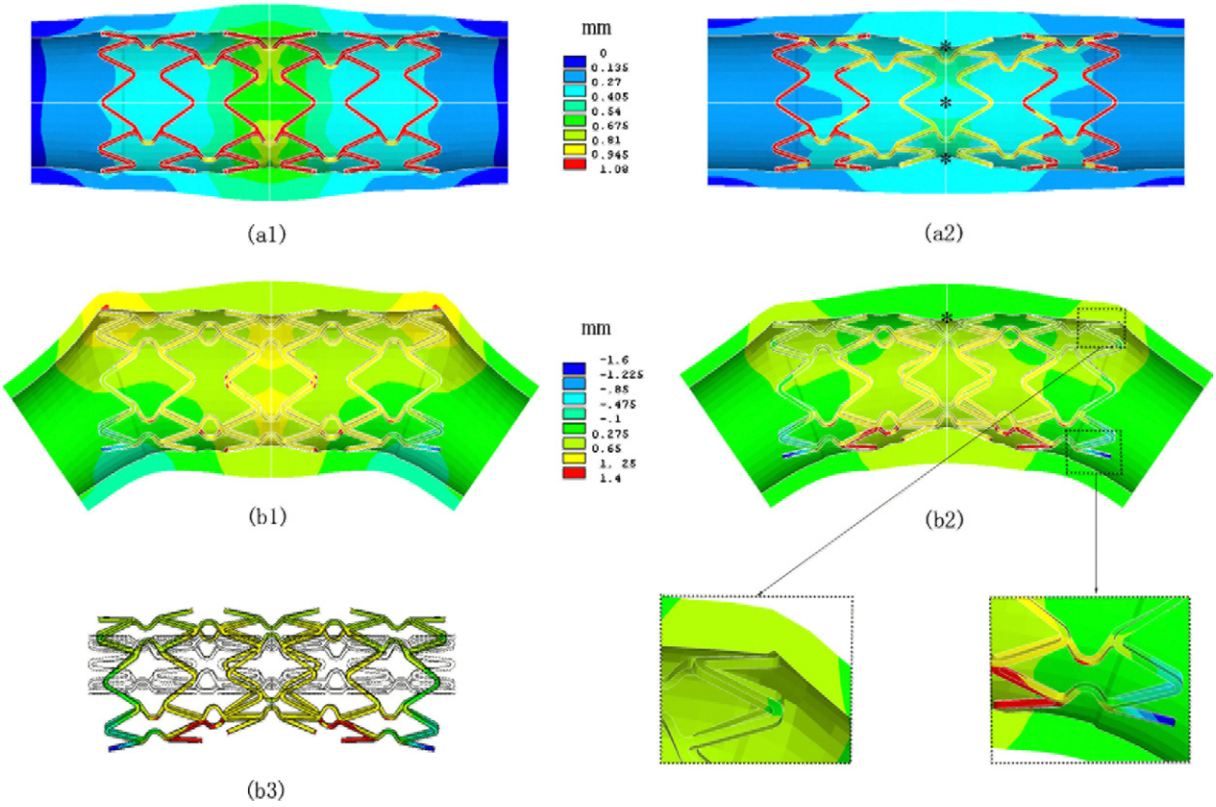

Fig. 3. Deformation configuration of the SV and CV model. (a1) and (b1) Radial displacement of the SV model and the CV model (based on LTCS), respectively, when the balloon was expanded to 3.3 mm and a pressure of 0.0133 MPa was loaded on the inner faces of the tissue. (a2) and (b2) Radial displacement of the SV model and the CV model, respectively, when the balloon was retracted and the vessel was only scaffolded by the stent. Insets of (b2) show the details of deformation at stent extremes of the CV model. The symbols "*" in (a2) and (b2) indicate the locations of the maximum tissue prolapse between stent struts of the SV model and the CV model, respectively. (b3) The stent in the CV model was bent by the tissue after the balloon was retracted; and its original shape edge is also shown for comparison.

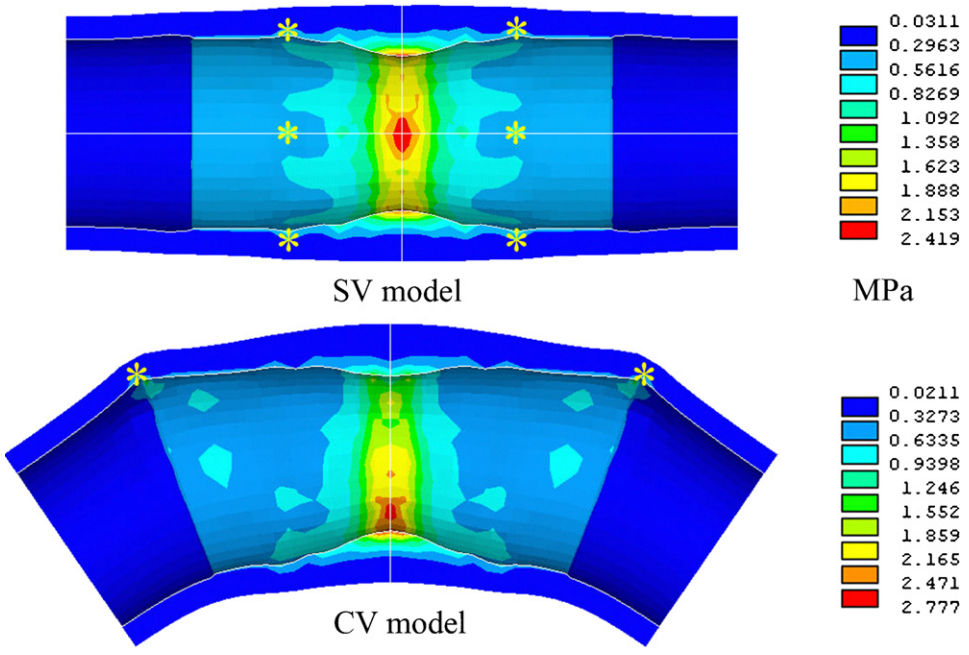

Fig. 4. First principal stress distribution on the plaque and vessel in the SV and CV model, which reflects the tensile stress in the tissue caused by stenting. The symbols "*" indicate the locations of highest vessel stress area for the SV model (0.174 MPa) and the CV model (0.517 MPa).

restenosis (Lally et al., 2005). The non-conformity of hinge points also indirectly caused the stent extreme departure form the vessel at inner curvature. For drug-eluting stents, this part of vessel may be hardly influenced by drugs.

Compared with the SV model, the final minimum lumen area of the CV model was decreased, which was partially the result of increased prolapse between struts. Excessive tissue prolapse can be attributed to acute thrombus (Farb et al., 2003) and restenosis (Hoffmann et al., 1996).

In terms of the physics of the CV model, stent bending is mainly attributed to tissue contact and link deformation. When the stent was bent, the links at outer curvature were stressed apart and links of inner curvature were compressed closer, which accords with the previous works (Perini et al., 2004; Mori and Saito, 2005). The non-conformity of the stent to vessel is mainly due to insufficient deformation of links, especially at stent extremes. The tissue at stent extremes is much softer than the middle tissue with severe stenosis, and the contact force to deform links was insufficient. So stent design should consider softer links at stent extremes. Furthermore, we propose if the balloon were designed to expand in similar curvature as the vessel, the stent could be bent in advance and conform to the vessel better.

The main limitation of the study is no consideration of fluent dynamics. ISR may be due to a complex combination of several factors. In fact, a flow effect on ISR may be larger than local mechanics of stent contact. As Fig. 3b2 shows, the non-conformity between the stent and the vessel could generate unwanted turbulence in the blood stream while favoring the creation of thrombosis. Moreover, curved tissue would cause severe flow disruption than straight vessel (Qiu and Tarbell, 2000). So the study of the fluent dynamics will be included in our future work.

In a conclusion, this three-dimensional FEM model provides a tool to study the interactions between stents and curved vessels. We offered some explanations for clinical reports about ISR in tortuous vessels using it and suggested relative stent and balloon designs. This method can test conformability of existing stents and help designers to devise novel stents for a coming drug-eluting stent era.

Acknowledgements

The authors are indebted to PhD Koji Mori, from Yamaguchi University, Japan for his direction and advices. This work was financially supported by the National High Technology Research and Development Program (No. 2002AA326010) and the National Natural Science Foundation of China (No. 50471066).

References

Abhyankar, A.D., Luyue, G., Bailey, B.P., 1997. Stent implantation in severely angulated lesions: safety, efficacy, and morphological remodeling. Catheterization and Cardiovascular Diagnosis 40, 261–264.

ANSYS documentations. ANSYS Release 9.0, 2004.

Brand, M., Ryvkin, M., 2005. The cardiocoil stent–artery interaction. Journal of Biomechanical Engineering—Transactions of the ASME 127, 337–344.

Chen, M.C.Y., Lu, P.-C., Chen, J.S.Y., et al., 2005. Computational hemodynamics of an implanted coronary stent based on three-dimensional cine angiography reconstruction. American Society of Artificial Internal Organs Journal 51, 313–320.

Colombo, A., Stankovic, G., Moses, J.W., 2002. Selection of coronary stents. Journal of the American College of Cardiology 40, 1021–1033.

Farb, A., Burke, A.P., Kolodgie, F.D., et al., 2003. Pathological mechanisms of fatal late coronary stent thrombosis in humans. Circulation 108, 1701–1706.

Hoffmann, R., Mintz, G.S., Dussaillant, G.R., et al., 1996. Patterns and mechanisms of in-stent restenosis: a serial intravascular ultrasound study. Circulation 94, 1247–1254.

Holzapfel, G.A., Stadlr, M., Gasser, T.C., 2005. Changes in the mechanical environment of stenotic arteries during interaction with stents: computational assessment of parametric stent designs. Journal of Biomechanical Engineering—Transactions of the ASME 127, 166–180.

Johnston, B.M., Johnston, P.R., Corney, S., et al., 2006. Non-Newtonian blood flow in human right coronary arteries: transient simulations. Journal of Biomechanics 39, 1116–1128.

Kalmar, G., Hubner, F., Voelker, W., et al., 2002. Radial force and wall apposition of balloon-expandable vascular stents in eccentric stenoses: an in vitro evaluation in a curved vessel model. Journal of Vascular and Interventional Radiology 13, 499–508.

LaDisa, J.F., Olson, L.E., Guler, I., et al., 2005. Circumferential vascular deformation after stent implantation alters wall shear stress evaluated with time-dependent 3D computational fluid dynamics models. Journal of Applied Physiology 98, 947–957.

Lally, C., Dolan, F., Prendergast, P.J., 2005. Cardiovascular stent design and vessel stresses: a finite element analysis. Journal of Biomechanics 38, 1574–1581.

Lee, R.T., 2000. Atherosclerotic lesion mechanics versus biology. Zeitschrift für Kardiologie 89, S080–S084.

Liao, R., Green, N.E., Chen, S.Y.J., et al., 2004. Three-dimensional analysis of in vivo coronary stent–coronary artery interactions. International Journal of Cardiovascular Imaging 20, 305–313.

Mitra, A.K., Agrawal, D.K., 2006. In stent restenosis: bane of the stent era. Journal of Clinical Pathology 59, 232–239.

Mori, K., Saito, T., 2005. Effects of stent structure on stent flexibility measurements. Annals of Biomedical Engineering 33, 733–742.

Natarajan, S., Mokhtarzadeh-Dehghan, M.R., 2000. A numerical and experimental study of periodic flow in a model of a corrugated vessel with application to stented arteries. Medical Engineering and Physics 22, 555–566.

Perini, L., Migliavacca, F., Auricchio, F., et al., 2004. Numerical investigation of the intravascular coronary stent flexibility. Journal of Biomechanics 37, 495–501.

Phillips, P.S., Alfonso, F., Segovia, J., et al., 1997. Effects of Palmaz–Schatz stents on angled coronary arteries. American Journal of Cardiology 79, 191–193.

Prendergast, P.J., Lally, C., Daly, S., et al., 2003. Analysis of prolapse in cardiovascular stents: a constitutive equation for vascular tissue and finite element modelling. Journal of Biomechanical Engineering—Transactions of the ASME 125, 692–699.

Qiu, Y., Tarbell, J.M., 2000. Numerical simulation of pulsatile flow in a compliant curved tube model of a coronary artery. Journal of Biomechanical Engineering—Transactions of the ASME 122, 77–85.

Rieu, R., Barragan, P., Garitey, V., et al., 2003. Assessment of the trackability, flexibility, and conformability of coronary stents: a comparative analysis. Catheterization and Cardiovascular Interventions 59, 496–503.

Tanabe, K., Serruys, P.W., Grube, E., et al., 2003. TAXUS III trial—in-stent restenosis treated with stent-based delivery of paclitaxel

incorporated in a slow-release polymer formulation. Circulation 107, 559–564.

Wang, W.-Q., Liang, D.-K., Yang, D.-Z., et al., 2006. Analysis of the transient expansion behavior and design optimization of coronary stents by finite element method. Journal of Biomechanics 39, 21–32.

Wentzel, J.J., Whelan, D.M., van der Giessen, W.J., et al., 2000. Coronary stent implantation changes 3-D vessel geometry and 3-D shear stress distribution. Journal of Biomechanics 33, 1287–1295.

Yang, D.-Z., 2001. A kind of coronary stent. China patent 00263981.5. 2001 October 17.

Zhou, R.-H., Lee, T.-S., Tsou, T.-C., et al., 2003. Stent implantation activates Akt in the vessel wall: role of mechanical stretch in vascular smooth muscle cells. Arteriosclerosis, Thrombosis, and Vascular Biology 23, 2015–2020.

Zhu, H., Warner, J.J., Gehrig, T.R., et al., 2003. Comparison of coronary artery dynamics pre- and post-stenting. Journal of Biomechanics 36, 689–697.